A Controller for Si MZI-Based Spanke-Benes Optical Switch Fabric With Automatic Calibration Capability

Hyun-Kyu Kim , *Graduate Student Member, IEEE*, Yongjin Ji , Kihun Kim, and Woo-Young Choi , *Member, IEEE*

Abstract—We demonstrate an FPGA-based controller for Si MZI-based Spanke-Benes 4×4 optical switch fabric that can automatically calibrate each individual switching cell and select the desired routing configuration. In order to minimize the power consumption for optical switching operation, the optimal heater voltages for the cross and the bar state of each switching cell is determined during the calibration. The operation of our controller is successfully verified with a Si MZI-based Spanke-Benes 4×4 optical switch.

Index Terms—Optical switch calibration, optical switch fabric, Si mach-zehnder interferometer (MZI), Spanke-Benes.

I. INTRODUCTION

THE wide spread of mobile services, high-definition video streaming, and AI-based services is significantly increasing the amount of data traffic in data centers, resulting in the exponential increase in the total bandwidth required in data center networks. In order to keep up with this bandwidth increase, many electrical wireline interfaces within data centers are being replaced with optical interconnects. Additionally, there is a growing interest in the optical switch fabric that enables complete optical domain routing [1], [2], [3]. Among these, the optical switch fabric based on the Si photonic platform is gaining attention because it can provide high performance in a cost-effective manner provided by the well-established Si fabrication technology [4], [5], [6]. Furthermore, Si-based optical switch fabric can be used for other emerging applications such as photonic FPGAs [7], quantum computing [8], [9], machine learning accelerators [10], and photonic neural networks [11].

Most optical switch fabrics rely on non-blocking switches that enable flexible I/O assignment. Fig. 1 shows examples of non-blocking optical switch configurations such as Benes [12], Spanke-Benes [13], and more recently reported PILOSS structure [14]. 4×4 configuration is shown in the figure for simplicity. Each structure has its own advantages and disadvantages. Benes architecture is widely used in switching networks due to its simple structure. However, as the number of ports increases, the number of waveguide crossings increases significantly. PILOSS architecture has the uniform loss characteristics,
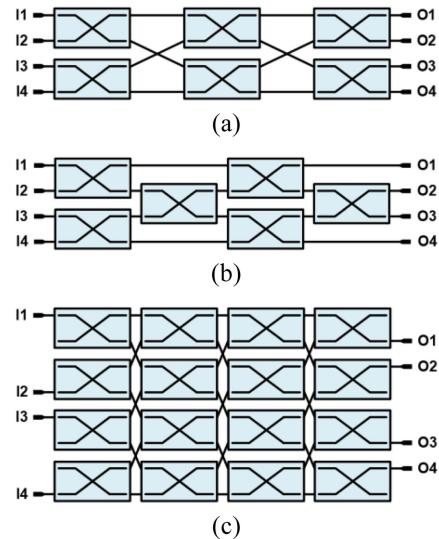

Fig. 1. Block diagrams of 4×4 switch fabric, (a) benes (b) spanke-benes (c) PILOSS structure.

but the power consumption of the calibration/control system can be very high since as many switching cells as the port number are required. In contrast, Spanke-Benes architecture has no waveguide crossings and can provide reduced calibration/control power consumption since it has fewer switching cells, although it suffers from the non-uniform loss characteristics. In this study, we select the Spanke-Benes configuration as our target optical switch fabric for which an electronic controller is implemented.

To efficiently control the optical switch fabric, there is a need for energy-efficient electronic controllers. This is particularly important for large-capacity switching systems consist of numerous switching cells. Moreover, since there is unavoidable uncertainty in the initial state of each switching cell due to process variations in Si photonic integrated circuit (PIC) fabrication, a calibration technique is required with which the initial state of each switch is monitored. Various techniques for automated calibration of the optical switch fabric have been reported. In [15], the approximation and predictive search method is used for automatic calibration of 32×32 Si MZI-based PILOSS optical switch fabric, which can significantly reduce calibration time. However, the heater power required for the π phase shift must be known in advance and the linear heater driver operation is necessary as the operating power of another state is calculated by adding P_π to the operating power of one state. [16] proposes

the automatic calibration technique for 4×4 Si MZI-based Benes optical switch fabric, in which the individual switching cell is calibrated with multiple laser inputs and measuring all the output ports. Since the output signals are summed during calibration in this method, the monitoring signal quality can be improved. However, using all the output ports for calibrating each switching cell can increase the complexity of the monitoring system. Some optical systems utilize complex calibration methods using machine learning [17] or iteration algorithm [18] techniques, which can be an excellent solution especially for large-scale systems. However, they typically require a significant amount of computation, which may not be desirable for certain applications.

In this article, we demonstrate an electronic control system based on FPGA that performs the initial calibration in which the minimum heater voltage required for the cross or the bar state is determined for each switching cell. This article is organized as follows. Section II discusses the calibration scheme for Si MZI-based 4×4 optical switches and how it can be extended to larger systems. Section III explains the implemented control system and presents the measurement results. Section IV gives the conclusion.

II. CALIBRATION SCHEME

Switching cells used in the Si-based optical switch fabric include Mach-Zehnder Interferometers (MZI) [19], ring-resonators [20], MEMS [21], and photonic crystals [22]. Among these, the MZI-based optical switch is often used due to its simplicity and relative robustness against temperature variation. An MZI switching cell having two 3-dB directional couplers as shown in Fig. 2(a) should be in the cross state if both arms are of the same length. In order to convert this into a bar state, one MZI arm can be heated. However, the process variation that occurs during fabrication causes the length and/or the effective index difference between two arms unknown, making the initial switching cell state uncertain and thus requiring calibration.

Fig. 2(b) shows how the output optical power at the cross port, represented by T in Fig. 2(a), changes when either top heater or bottom heater is heated. The red curve represents T when the top heater is heated by the amount of P_{UP} and the blue curve represents T when the bottom heater is heated by the amount of P_{DN}. The MZI switching cell is in the cross-state when $T = T_{max}$ and in the bar-state when $T = T_{min}$ as shown in the figure. With the process variation, the initial state of the switch when no heating nor bias is applied cannot be predicted and, consequently, a certain amount of P_{UP} or P_{DN} is needed to bring the switch to the cross or the bar state. For this, depending on the initial state, selecting the up or the down heater can save heater power. For example, for the case shown in Fig. 2(b), the up heater should be used for bringing the switching cell to the cross state as $P_{UP,cross} < P_{DN,cross}$ and the down heater for the bar state as $P_{DN,bar} < P_{UP,bar}$. For the case shown in Fig. 2(c), the down heater should be used for the cross state and the up heater for the bar state. To determine the required P_{UP} or P_{DN}, both heater powers are scanned and the optimal P_{UP} and P_{DN} values are identified and stored during calibration, and used for switching operation.
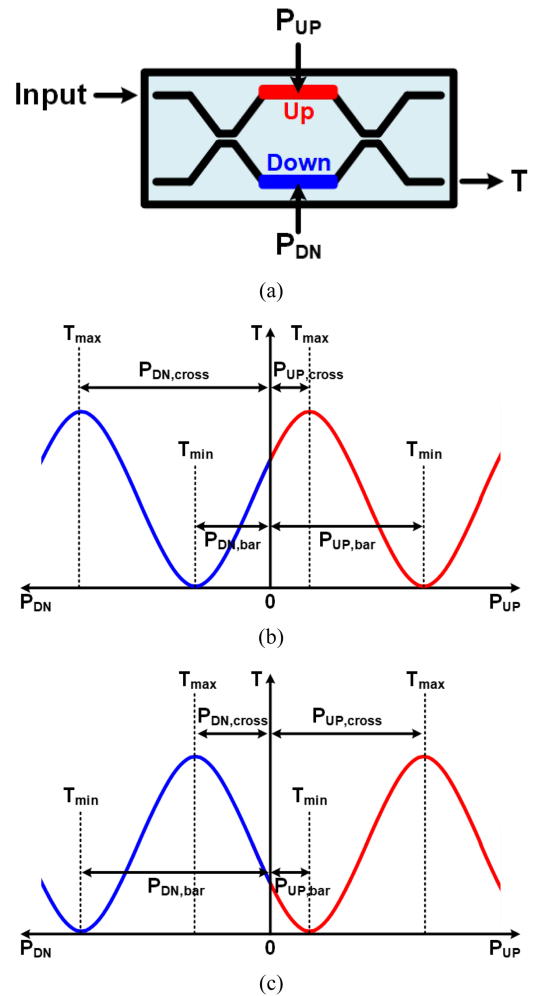

Fig. 2. (a) MZI-based cross-bar switch having 3-dB directional couplers with 2 heaters. (b), (c) cross-state output power characteristics with two different initial condition.

To apply the above calibration method to the Spanke-Benes optical switch fabric, sequential calibration of individual switching cells is required. For this, it is desirable if the number of the input and output ports used for calibration can be reduced as much as possible. For the 4×4 Spanke-Benes optical switch fabric, initially any input port can be selected, for example, In-1 in Fig. 3(a). Then, the output monitoring port of Out-4 is selected so that the resulting monitoring path shown in red line in Fig. 3(a) contains three switching elements, SW1, SW3, and SW5. Although their states are unknown, there is a good possibility that the optical power monitored at Out-4 is sufficient enough for performing calibration of SW1 in the manner described above. Then, the SW1 state can be brought to the cross state so that the monitoring power at Out-4 can be maximized, and SW3 is calibrated. After this, SW3 is brought to the cross state and SW5 is calibrated. If the monitored output power at Out-4 is not large enough because any of SW1, SW3 or SW5 is initially in the bar state, then another monitoring path with a different output port can be used. Because the input power should come out at output ports except the loss, more than one monitoring path can be created for one input regardless of the initial state of switching cells. For example, monitoring paths consisting of SW1 (bar),
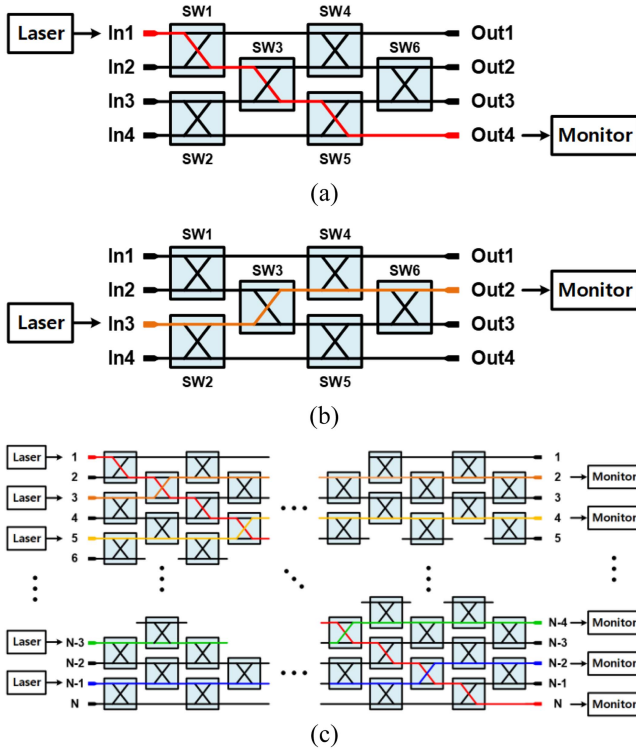
(a)

(b)

(c)

Fig. 3. (a) Example of I/O placement and its first monitoring path for 4×4 spanke-benes optical switch fabric and (b) its second monitoring path. (c) $N \times N$ example of I/O placement and its monitoring path.

SW4 (cross), SW6 (bar) states with Out-2, or SW1 (cross), SW3 (bar), SW4 (cross) with Out-1 can be used for calibrating three switching cells. Once three switching cells are calibrated in this manner, the remaining three switching cells can be calibrated by using a different input port. For example, after calibrating SW1, SW3 and SW5, the laser source can be moved to In-3 as shown in Fig. 3(b), and SW2, SW4, and SW6 can be calibrated.

Above sequential calibration scheme can be in principle extended to $N \times N$ as shown in Fig. 3(c), where N is a multiple of 2. In this case, N/2 input ports have to be used, and for each input port, N-1 switching cells can be calibrated. In addition, this calibration method can be also applied to any non-blocking switch architecture such as Benes or PILOSS switches.

III. CALIBRATION AND CONTROL DEMONSTRATION

To demonstrate the feasibility of our calibration system, a Si MZI-based 4×4 Spanke-Benes optical switch fabric is implemented. Fig. 4 shows the fabricated chip microphotograph. It is realized with the Si Photonics fabrication process on 220-nm SOI provided by Applied Nanotools. All switching cells are based on the MZI having nominal 300-μm arm length with two Ti-W metal heaters located above two MZI arms. Grating couplers are used for input and output optical coupling. The resistance of the built-in heater is 337-Ω and each MZI can consume up to 47-mW for calibration, which corresponds to the $P_{2\pi}$.

Fig. 5(a) and (b) shows the measured normalized characteristic curves obtained for each switching cell in the fabricated 4×4 optical switch fabric. For these measurements, I/O placement
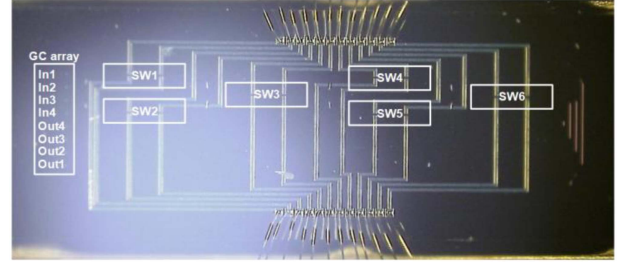

Fig. 4. Chip microphotograph of fabricated Si MZI-based 4×4 spanke-benes optical switch fabric.
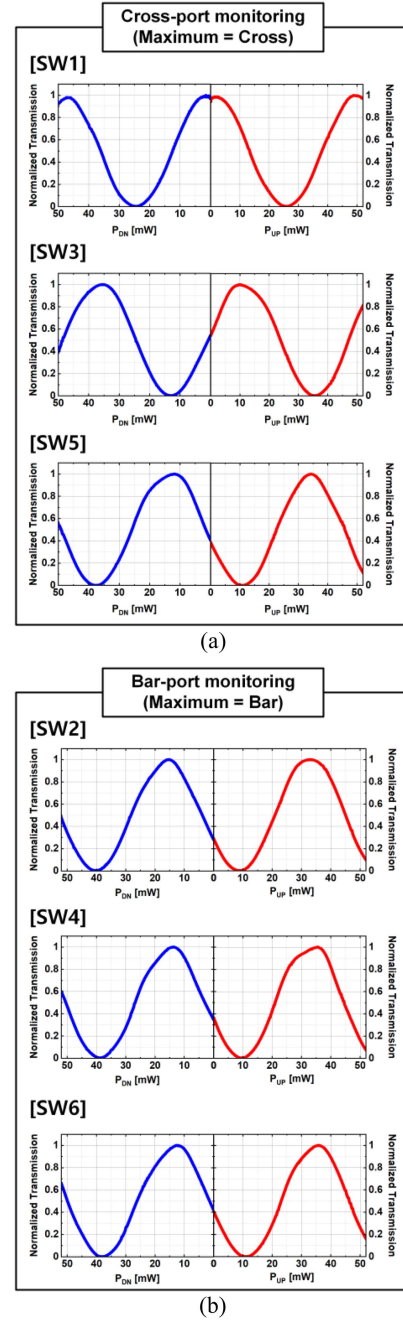

(a)

(b)

Fig. 5. Measured normalized characteristic curves of each MZI switching cells in fabricated 4×4 optical switch fabrics for (a) SW1, SW3, SW5 and (b) SW2, SW4, SW6.
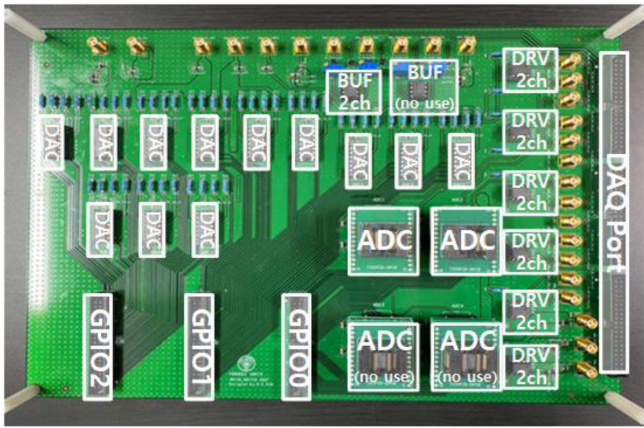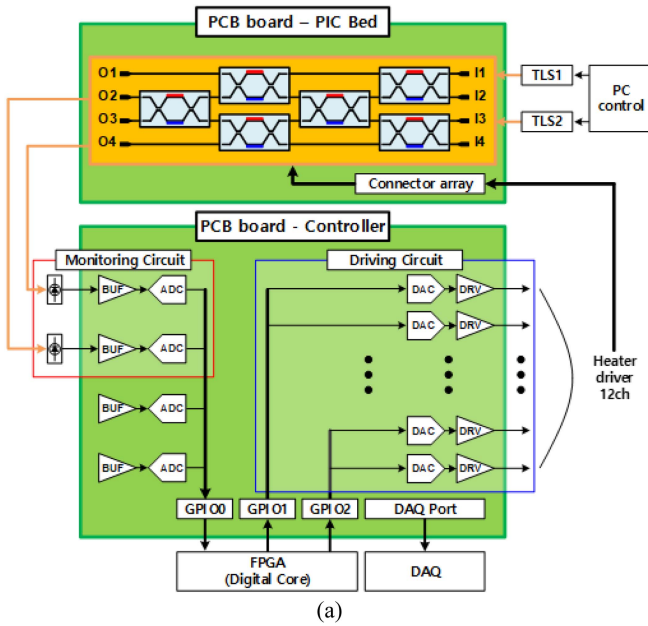
Fig. 6. (a) Block diagram of designed calibration system for 4 × 4 spanke-benes optical switch fabric (b) and its PCB board implementation.

Fig. 7. (a) Timing diagram of MZI-based optical switch calibration scheme. (b) Measurement result of MZI switching cell calibration process.

and monitoring paths shown in Fig. 3(a) and (b) were used. By measuring the output power while scanning P_{UP} and P_{DN} for the target switching cell, the MZI characteristics were measured.

An electronic control board is realized on the standard FR4 PCB, which contains circuits for output port monitoring and driving circuits for the heaters. Fig. 6(a) shows the block diagram of the controller, which is implemented with an FPGA for the digital core, buffer/ADC for monitoring circuits, and DAC/driver for driving circuits. Through GPIOs on the PCB board, the FPGA processes the digital bits used for the monitoring circuit and the driving circuit. The monitoring circuit converts the PD current into the voltage (V_{PD}) and then into 8-bit digital codes through the unity-gain buffer and 25-MS/s ADC. The driving circuit converts the 12 6-bit parallel data bus from the FPGA into the driving voltage through 12 DACs and drives the heaters through a unity-gain driver having bandwidth of 2.7-MHz.
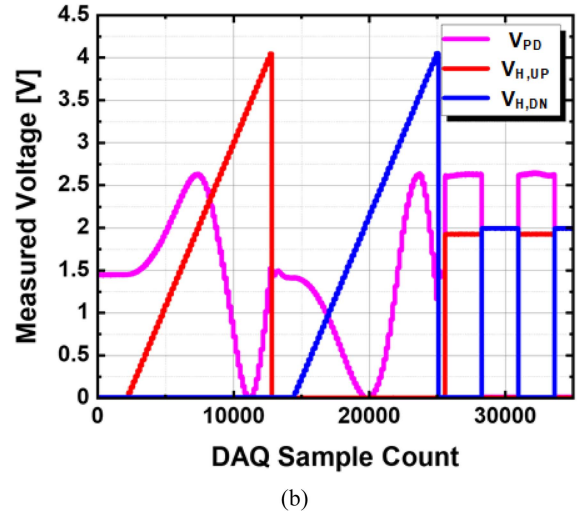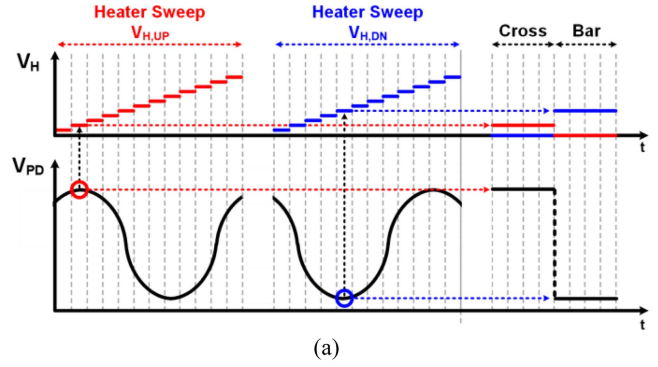
The calibration flow of MZI-based optical switch implemented in FPGA is shown in Fig. 7(a). First, a voltage sweep is performed at intervals of 62.5-mV up to 4-V for the heater of each arm. During this process, the points where the monitoring value becomes the maximum and the minimum are found and the corresponding DAC codes are saved. After that, the DAC codes of two heaters for the cross-state are compared, and the one with the smaller code is stored for the cross-state operation. The other heater is used for the bar-state operation.

As an example of its operation, Fig. 7(b) shows heater voltages applied to SW3 as well as the monitored PD output signal for the monitoring path shown in Fig. 3(a). For this measurement, SW1 and SW5 are placed in the cross state. 8-dBm, 1540-nm C-band tunable laser source (TLS) is used for the input source. The sample rate of data acquisition (DAQ) is 1-kHz. After calibration is done, the switch is brought to the cross state and the bar state so that the calibration results can be confirmed.

Fig. 8 shows the measurement results of the sequential calibration of 4 × 4 Spanke-Benes optical switch fabric. The experimental environment is the same as the calibration verification of a single switching cell, except for TLS output power is set to 5-dBm. Fig. 8(a) shows the result obtained during the calibration using the monitoring path shown in Figs. 3(a) and 8(b) using the monitoring path shown in Fig. 3(b). For our controller, the
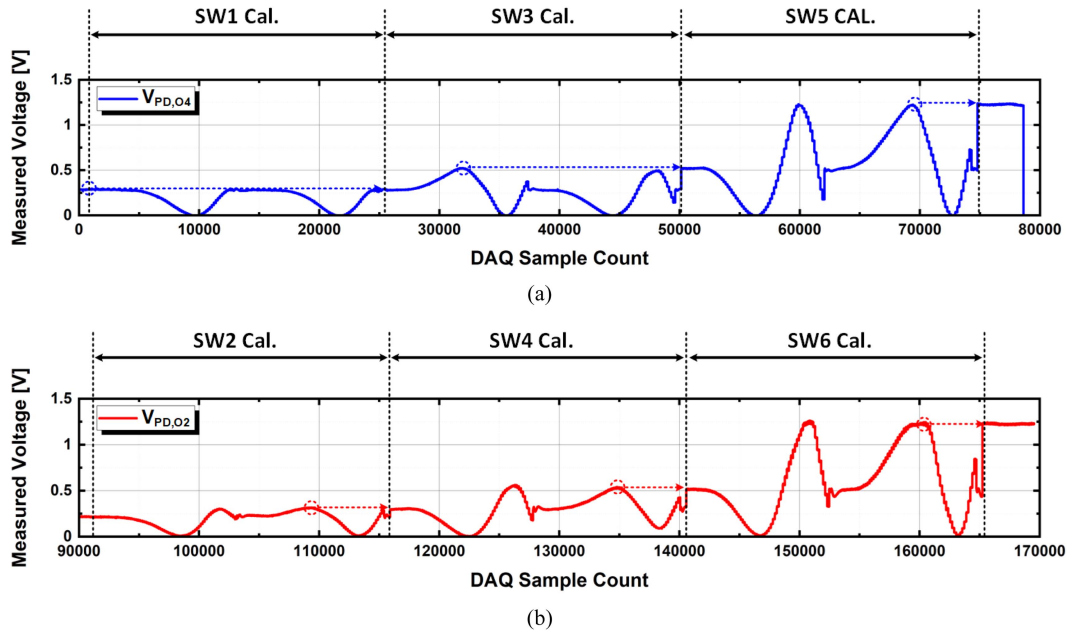
Fig. 8.   Measurement result of sequential calibration process of 4 × 4 spanke-benes optical switch fabric obtained from (a) the monitoring path passing through SW1, SW3, SW5 and (b) SW2, SW4, SW6.
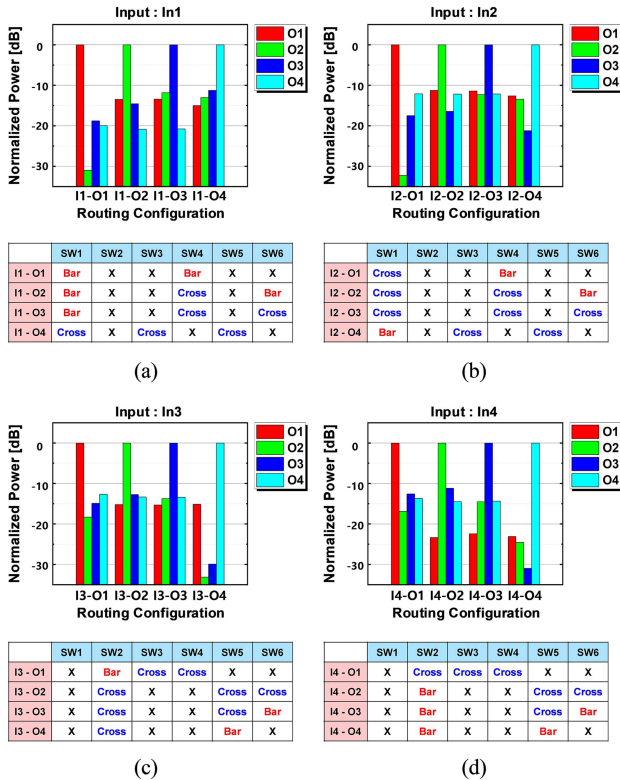

Fig. 9.   Measured output optical power of output ports for given routing configuration of calibrated optical switch fabric for (a) In-1, (b) in-2, (c) in-3 and (d) in-4.

minimum optical power at the monitoring output port required for calibration is about −25.7-dBm. Fig. 9 shows the measured power for every possible routing condition realized with the controller after the calibration. The x-axis represents applied

input-output configuration, and y-axis the normalized power measured at each output port identified with the different. Below each figures, the cross-bar states of the individual switching cells for each routing configurations are specified, which X mark means don't care. The range of measured crosstalk suppression is 10.68-dB to 32.53-dB.

IV. CONCLUSION

We present an electronic controller the for Si-MZI based Spanke-Benes 4 × 4 optical switch fabric. The controller is capable of monitoring the initial state of the MZI switching cell and determines which heater to use for the cross or the bar operation for the minimum power consumption. It can also perform sequential calibration of individual switching cells with the minimum calibration cost. We experimentally demonstrate the controller can correctly calibrate and properly route signals for 4 × 4 Si MZI-based Spanke-Benes optical switch fabric.

ACKNOWLEDGMENT

REFERENCES

[1] F. Yan, X. Xue, and N. Calabretta, "HiFOST: A scalable and low-latency hybrid data center network architecture based on flow-controlled fast optical switches," *J. Opt. Commun. Netw.*, vol. 10, no. 7, pp. 1–14, Jul. 2018, doi: 10.1364/JOCN.10.0000B1.

[2] Q. Cheng, M. Bahadori, M. Glick, S. Rumley, and K. Bergman, "Recent advances in optical technologies for data centers: A review," *Optica*, vol. 5, no. 11, pp. 1354–1370, Oct. 2018, doi: 10.1364/OPTICA.5.001354.

[3] W. Hou, P. Guo, L. Guo, X. Zhang, H. Chen, and W. Liu, "O-Star: An optical switching architecture featuring mode and wavelength-division multiplexing for on-chip many-core systems," *J. Lightw. Technol.*, vol. 40, no. 1, pp. 24–36, Jan. 2022, doi: 10.1109/JLT.2021.3119564.

[4] X. Chen, J. Lin, and K. Wang, "A review of silicon-based integrated optical switches," *Laser Photon. Rev.*, vol. 17, no. 4, Apr. 2023, Art. no. 2200571, doi: 10.1002/lpor.202200571.

[5] B. G. Lee and N. Dupuis, "Silicon photonic switch fabrics: Technology and architecture," *J. Lightw. Technol.*, vol. 37, no. 1, pp. 6–20, Jan. 2019, doi: 10.1109/JLT.2018.2876828.

[6] T. J. Seok, K. Kwon, J. Henriksson, J. Luo, and M. C. Wu, "Wafer-scale silicon photonic switches beyond die size limit," *Optica*, vol. 6, no. 4, pp. 490–494, Apr. 2019, doi: 10.1364/OPTICA.6.000490.

[7] W. Bogaerts et al., "Programmable photonic circuits," *Nature*, vol. 586, pp. 207–216, Oct. 2020, doi: 10.1038/s41586-020-2764-0.

[8] J. M. Arrazola et al., "Quantum circuits with many photons on a programmable nanophotonic chip," *Nature*, vol. 591, pp. 54–60, Mar. 2021, doi: 10.1038/s41586-021-03202-1.

[9] X. Yan et al., "Silicon photonic quantum computing with spin qubits," *APL Photon.*, vol. 6, Jul. 2021, Art. no. 070901, doi: 10.1063/5.0049372.

[10] B. J. Shastri et al., "Photonics for artificial intelligence and neuromorphic computing," *Nature Photon.*, vol. 15, pp. 102–114, Feb. 2021, doi: 10.1038/s41566-020-00754-y.

[11] L. De Marinis, M. Cococcioni, P. Castoldi, and N. Andriolli, "Photonic neural networks: A survey," *IEEE Access*, vol. 7, pp. 175827–175841, 2019, doi: 10.1109/ACCESS.2019.2957245.

[12] L. Lu, L. Zhou, Z. Li, X. Li, and J. Chen, "Broadband 4 × 4 non-blocking silicon electrooptic switches based on Mach–Zehnder interferometers," *IEEE Photon. J.*, vol. 7, no. 1, Feb. 2015, Art. no. 7800108, doi: 10.1109/JPHOT.2015.2390195.

[13] D. Zheng, J. - D. Domenech, W. Pan, X. Zou, L. Yan, and D. Perez, "Low-loss broadband 5 × 5 non-blocking Si_3N_4 optical switch matrix," *Opt. Lett.*, vol. 44, no. 11, pp. 2629–2632, May 2019, doi: 10.1364/OL.44.002629.

[14] K. Suzuki et al., "Ultra-compact 8 × 8 strictly-non-blocking Si-wire PILOSS switch," *Opt. Exp.*, vol. 22, no. 4, pp. 3887–3894, Feb. 2014, doi: 10.1364/OE.22.003887.

[15] S. Suda et al., "Fast and accurate automatic calibration of a 32 × 32 silicon photonic strictly-non-blocking switch," in *Proc. Adv. Photon.*, 2017, Paper PTu3C.5, doi: 10.1364/PS.2017.PTu3C.5.

[16] Y. Huang, Q. Cheng, N. C. Abrams, J. Zhou, S. Rumley, and K. Bergman, "Automated calibration and characterization for scalable integrated optical switch fabric without built-in power monitors," in *Proc. Eur. Conf. Opt. Commun.*, 2017, pp. 1–3, doi: 10.1109/ECOC.2017.8345829.

[17] S. Pai et al., "Power monitoring in a feedforward photonic network using two output detectors," *Nanophotonics*, vol. 12, no. 5, pp. 985–991, Jan. 2023, doi: 10.1515/nanoph-2022-0527.

[18] V. Cimini et al., "Calibration of multiparameter sensors via machine learning at the single-photon level," *Phys. Rev. Appl.*, vol. 15, no. 4, Apr. 2021, Art. no. 044003, doi: 0.1103/PhysRevApplied.15.044003.

[19] L. Sanchez, A. Griol, S. Lechago, A. Brimont, and P. Sanchis, "Low-power operation in a silicon switch based on an asymmetric Mach–Zehnder interferometer," *IEEE Photon. J.*, vol. 7, no. 2, Apr. 2015, Art. no. 6900308, doi: 10.1109/JPHOT.2015.2407317.

[20] Q. Zhu et al., "Automated wavelength alignment in a 4 × 4 silicon thermo-optic switch based on dual-ring resonators," *IEEE Photon. J.*, vol. 10, no. 1, Feb. 2018, Art. no. 6600311, doi: 10.1109/JPHOT.2018.2791561.

[21] N. Quack et al., "MEMS-enabled silicon photonic integrated devices and circuits," *IEEE J. Quantum Electron.*, vol. 56, no. 1, Feb. 2020, Art. no. 8400210, doi: 10.1109/JQE.2019.2946841.

[22] D. M. Beggs, T. P. White, L. Cairns, L. O'Faolain, and T. F. Krauss, "Ultrashort photonic crystal optical switch actuated by a microheater," *IEEE Photon. Technol. Lett.*, vol. 21, no. 1, pp. 24–26, Jan. 2009, doi: 10.1109/LPT.2008.2008104.